*metals*

MDPI

*Article*

# The Influence of Particle Shape, Powder Flowability, and Powder Layer Density on Part Density in Laser Powder Bed Fusion

**Lukas Haferkamp [1,2,*], Livia Haudenschild [2], Adriaan Spierings [1], Konrad Wegener [2], Kirstin Riener [3,4], Stefan Ziegelmeier [3] and Gerhard J. Leichtfried [4]**

[1] Inspire, Innovation Center for Additive Manufacturing Switzerland (ICAMS), Lerchenfeldstrasse 3, 9014 St. Gallen, Switzerland; spierings@inspire.ethz.ch
[2] ETH Zürich, Institute of Machine Tools and Manufacturing (IWF), Leonhardstrasse 21, 8092 Zürich, Switzerland; livia@haudenschild.com (L.H.); wegener@iwf.mavt.ethz.ch (K.W.)
[3] BMW Group FIZ, Knorrstraße 147, 80788 Munich, Germany; Kirstin.Riener@bmw.de (K.R.); Stefan.Ziegelmeier@bmw.de (S.Z.)
[4] Department of Mechatronics, Materials Science, Faculty of Engineering Science, University of Innsbruck, Technikerstrasse 13, 6020 Innsbruck, Austria; Gerhard.Leichtfried@uibk.ac.at
* Correspondence: haferkamp@inspire.ethz.ch

**Abstract:** The particle shape influences the part properties in laser powder bed fusion, and powder flowability and powder layer density (PLD) are considered the link between the powder and part properties. Therefore, this study investigates the relationship between these properties and their influence on final part density for six 1.4404 (316L) powders and eight AlSi10Mg powders. The results show a correlation of the powder properties with a Pearson correlation coefficient (PCC) of −0.89 for the PLD and the Hausner ratio, a PCC of −0.67 for the Hausner ratio and circularity, and a PCC of 0.72 for circularity and PLD. Furthermore, the results show that beyond a threshold, improvement of circularity, PLD, or Hausner ratio have no positive influence on the final part density. While the water-atomized, least-spherical powder yielded parts with high porosity, no improvement of part density was achieved by feedstock with higher circularities than gas-atomized powder.

**Keywords:** selective laser melting (SLM); laser powder bed fusion (LPBF); powder; particle size distribution; particle morphology; powder layer density; part density; flowability; Hausner ratio



**Citation:** Haferkamp, L.; Haudenschild, L.; Spierings, A.; Wegener, K.; Riener, K.; Ziegelmeier, S.; Leichtfried, G.J. The Influence of Particle Shape, Powder Flowability, and Powder Layer Density on Part Density in Laser Powder Bed Fusion. *Metals* **2021**, *11*, 418. https://doi.org/10.3390/met11030418

Academic Editor: Atila Ertas

Received: 25 January 2021
Accepted: 26 February 2021
Published: 4 March 2021



## 1. Introduction

The quality of parts produced by laser powder bed fusion (LPBF) is strongly influenced by feedstock material, which is the powder. The most important characteristics of powder for LPBF are usually considered to be the size distribution in [1], particle shape in [1,2], chemical composition in [3,4], flowability in [5], powder layer density (PLD) in [6,7], and the amount of internal porosity in [1]. Despite the significance of the raw material, there is a lack of quantified and broadly accepted powder requirements, which are unknown or, according to Tan et al. [2], often undisclosed by the powder suppliers for competitive reasons. Furthermore, there are no quantitative standards for LPBF powder published to date, which necessitates the identification of relevant powder characteristics and to quantify their influence on the LPBF process.

One powder characteristic that lacks quantified requirements is the particle shape. There are several production techniques for metal powders, including water-atomization (WA), gas-atomization (GA), plasma-atomization (PA), and centrifugal-atomization techniques as the plasma rotating electrode process (PREP), and mechanical milling [8]. The particle shape, however, varies across the different production techniques [2]. Currently,

GA powders are preferred in LPBF [2]. It is, however, unclear to what extent the powder particle shape affects processability and part quality in LPBF. Several studies

have shown the negative impact of non-spherical WA powder on the process and part quality [3,9,10]. It is, however, not clear, whether more spherical, e.g., PA and PREP powders, further improve part quality.

Several studies investigated the influence of the particle shape on part quality. Most of them were focused on a comparison of WA and GA powders. Riener et al. [11] compared the processing of three GA powders and one plasma-atomized AlSi10Mg powder. They concluded that, in general, higher part densities could be achieved by using more spherical powders. Brika et al. [12] investigated two PA powders and one GA Ti-6Al-4V powder and also found a positive influence of particle sphericity on the powder flowability and part density. Engeli et al. [3] investigated seven GA powders and one WA IN738LC powder for the LPBF process. They found higher porosity in the parts made of WA powder, which they attribute to its more irregular morphology. They also observed an influence of the Hausner ratio on part porosity of GA powders. Baitimerov et al. [13] processed three gas atomized AlSi12 powders and concluded that non-spherical particles lead to a low apparent density of the powder and thus porosity in the parts. Li et al. [9] processed one GA and one WA 1.4404 (316L) powder and found higher porosity in parts made from WA powder, which they attributed to its high oxygen content and low packing density. Hoeges et al. [10] compared the density of parts made from a single WA powder and a GA powder. They were able to process both powders to a density of more than 99%; however, the morphology, flowability, and chemical composition of the WA powder posed a challenge during processing on a LPBF machine. Irrinki et al. [14] investigated the processability of three WA powders and one GA 17-4-PH stainless steel powder and found that the GA powder generally yielded parts with less porosity, but were able to process the WA powder into parts with comparable densities and mechanical properties at sufficiently high energy densities. Jeon et al. [15] processed four Fe-powders, of which three were mixtures of spherical and non-spherical powders. They found an increase in the part porosity of blended powders for increasing size misfit between the spherical and non-spherical powders.

The literature indicates that spherical PA and PREP powders might, compared to less spherical GA powders, further improve part quality, especially final part density, which is, according to Hoeges et al. [10], one of the major quality metrics of LPBF. This paper therefore investigates the influence of the particle shape on the process with a focus on final part density. The PLD [5,9] and powder flowability [5,16] are often considered as a link between the powder and final part properties and are therefore measured for all powders in this experiment, as they allow inferring the densification mechanisms during LPBF. In contrast to previous studies, mostly GA, or more spherical, powders were used in this experiment. Thus, the results are more relevant for industrial practice, where mostly spherical powders are used [2,17].

## 2. Materials and Methods

### *2.1. Powder Characterization*

Six 1.4404 (316L) powders and eight AlSi10Mg powders were investigated. Their particle size distribution (PSD) was measured three times by laser diffraction with a LS230 laser diffractometer (Beckman Coulter, Inc., Brea, CA, USA) and the average PSD was used. The corresponding PSDs are displayed in Figure 1. The powder designation was chosen to reflect the alloy (Fe = 1.4404 (316L); Al = AlSi10Mg), the production process was as specified by the powder supplier (GA = gas-atomized; PREP = plasma rotating electrode process; WA = water-atomized; PA = plasma-atomized), and the volume-weighted D50 of a powder. The powders Fe-GA-38 and Fe-GA-47 as well as Fe-PREP-40 and Fe-PREP-47 were from the same powder batch and were separated into two powders by sieving. All other powders were from different batches. All powders were unused, as reuse of powder can change the powder properties, as discussed in [18]. A chemical influence can, however, not be entirely excluded, as the oxygen in the powder depends on the powder surface [19], which strongly depends on the PSD.

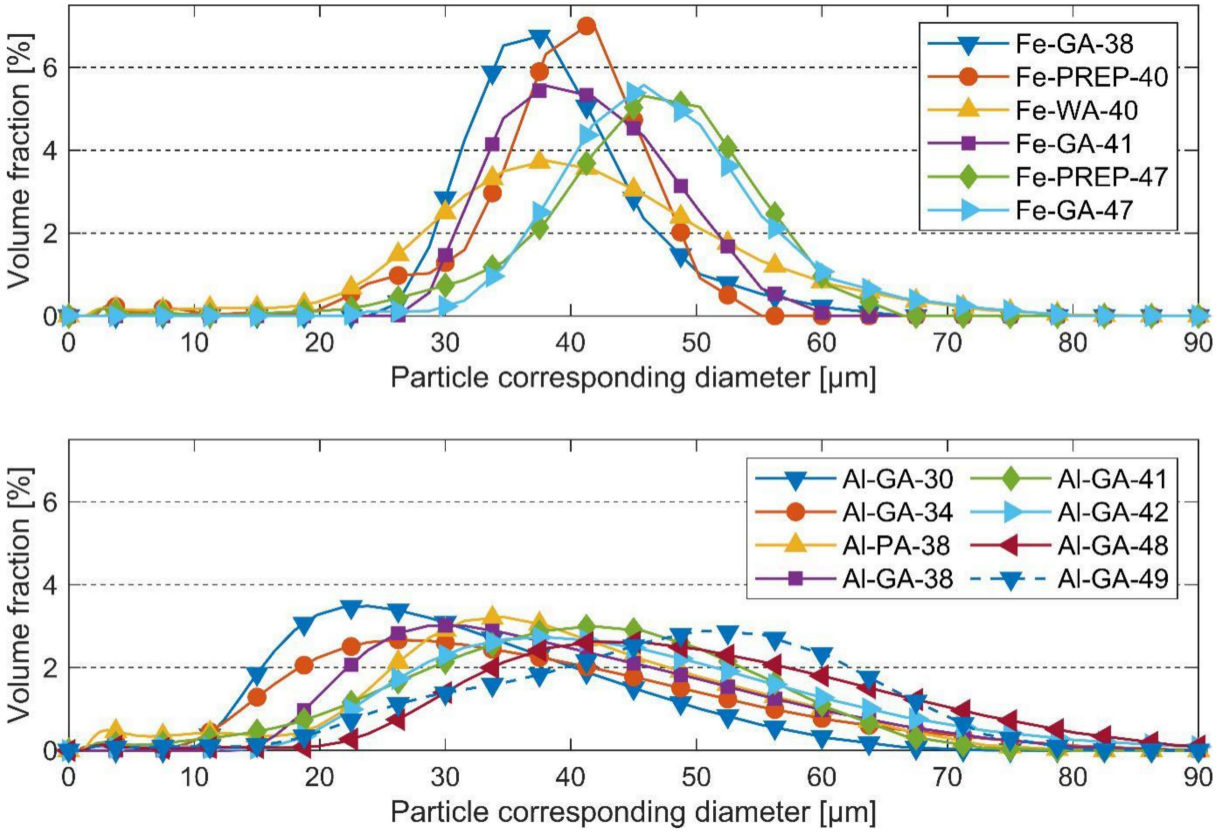


**Figure 1.** Particle size distribution (PSD) of the investigated powders: **top** 1.4404 (316L), **bottom** AlSi10Mg.

The particle shape factors were measured using a Leica DM6 light microscope (Leica Microsystems GmbH, Wetzlar, Germany). Images were taken by transmitted light microscopy and then processed in MATLAB (The MathWorks, Inc., Natick, MA, USA), where all agglomerates were manually removed until 3000 particles per powder were identified. The two commonly used shape factors, circularity and aspect ratio, were used in this study. The circularity $f_{circ}$ was calculated according to the equation used by Bouwman et al. [20] as $f_{circ} = (4\pi A)/P^2$, where $A$ is the area and $P$ the perimeter of the projected particle. The aspect ratio $f_{AR}$ was calculated as the ratio of the minimum Feret diameter $d_{fmin}$ to the maximum Feret diameter $d_{fmax}$ as $f_{AR} = d_{fmin}/d_{fmax}$. The apparent density $\rho_a$ and tap density $\rho_t$ of each powder were measured three times according to ASTM B417-18 [21] and ASTM B527-15 [22], respectively. The Hausner ratio, $H$, was then calculated as the ratio of the tap and apparent density as $H = \rho_t/\rho_a$.

### 2.2. Powder Layer Density Measurement

The PLD was measured by filling a cavity, as shown in Figure 2a, with a coating blade shown in Figure 2b. The PLD was then calculated from the powder mass and the known volume of the cavity. Two cavities were used, one with an average depth of 84.5 µm and the other with an average depth of 141.4 µm. Both were made from hardened 1.2379 steel with an outer cylinder diameter of 44.0 mm and a total height of 15.2 mm. The inner cavities with a diameter of 40 mm were produced by electrical discharge machining, and their depth was measured by a GelSight Benchtop system (GelSight, Inc., Waltham, MA, USA).

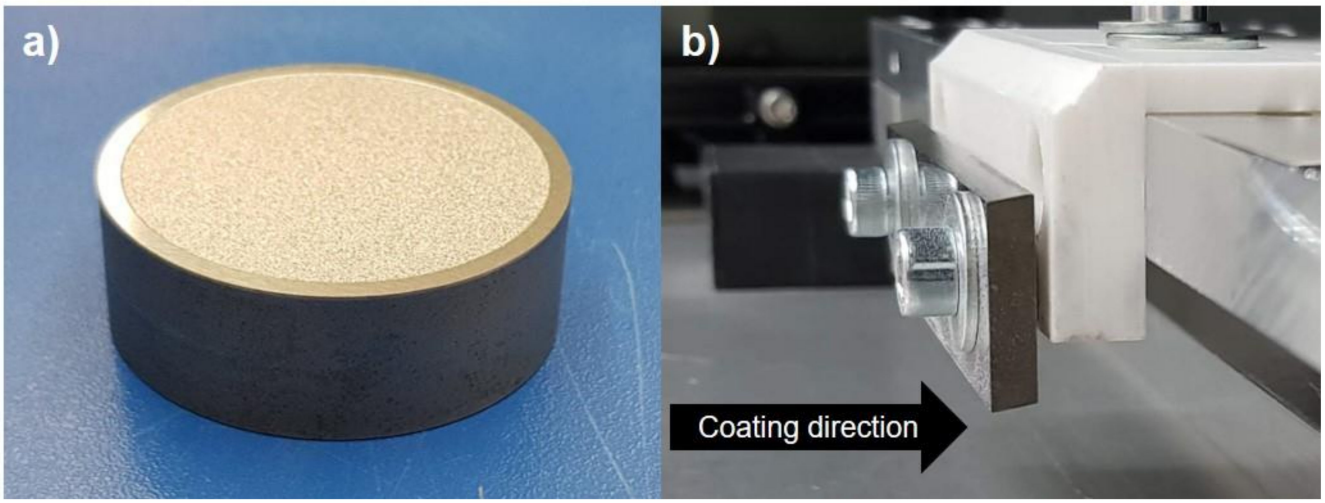


**Figure 2.** An (**a**) empty cavity and (**b**) coating blade from stainless steel.

The coating of the cavity was performed on a test bench, which was propelled with a toothed belt drive on the coater axis and a spindle screw drive on the *z*-axis. The cavity was placed on the *z*-platform and leveled such that the tip of the coating blade just touched the rim of the cavity along the entire movement on top of the cavity. The *z*-axis was then raised by 50 µm to create pressure between the coating blade and the rim of the cavity. This pressure ensured that no powder remained on the rim of the cavity after coating. The position of the cavity in the coating direction was secured with two mechanical stops on the z-platform.

The layer density of all powders was measured five times for each powder and cavity, thus moving the coating blade to its starting position in front of the *z*-platform. The cavity was then placed on the *z*-platform and the powder placement platform was placed around the cavity, as shown in Figure 3b. A powder with a volume of 12 $cm^3$ at apparent density was positioned in front of the cavity on the powder placement platform. The coater was then moved across the cavity at a speed of 100 mm/s. Eventually, the cavity was removed, cleaned from the outside, and weighed on an AX205 Delta Range scale by Mettler Toledo.

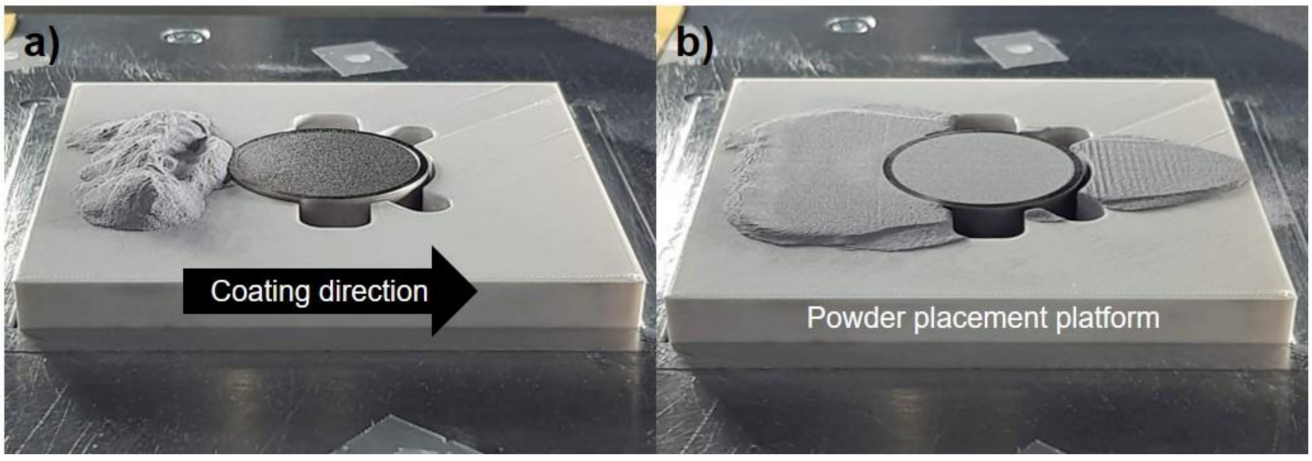


**Figure 3.** (**a**) Twelve $cm^3$ of powder placed in front of the cavity before the coating process, (**b**) powder in the cavity after the coating process.

### *2.3. Powder Processing*

All powders were processed on a Concept Laser M2 (Concept Laser GmbH, Lichtenfels, Germany) using the parameters listed in Table 1. Five 10 × 10 × 10 $mm^3$ cubes were built per scan speed, resulting in 25 cubes per build cycle. These cubes were evenly distributed

over the build plate to compensate for possible location-dependent differences in part density. The parts were not placed on a regular build plate, but with a custom-made insert to reduce the build chamber volume. This reduced the build platform to 95 mm in diameter. A brush was used for coating, which was different from the blade used for measuring PLD. This was done as the layer density measurement is only possible with a blade, whereas a build cycle with a blade would cause collisions of the steel blade during the processing of some powders. The density of final parts was measured using the Archimedes principle in acetone according to the procedure described by Spierings et al. [23]. Density as a quality metric was chosen as it is easy to measure and does directly influence the mechanical properties, as has been discussed in [11,24].

**Table 1.** Parameters used for processing.

| Parameter | Unit | Value |
|---|---|---|
| Laser power | (W) | 180 |
| Hatch | (µm) | 1.4404 (316L): 75, AlSi10Mg: 100 |
| Layer height | (µm) | 30 |
| Scan speed | (mm/s) | 1000, 1250, 1500, 1750, 2000 |
| Shielding gas | - | Nitrogen |
| Coating technology | - | Brush |
| Beam diameter (as measured) | (µm) | 105 |
| Coating speed | (mm/s) | 100 |
| Scanning strategy | - | 90° alternating, parallel to the sides of the cube, crosswise |

## 3. Results and Discussion

### *3.1. Circularity and Aspect Ratio*

Figure 4 shows the circularity and aspect ratio of all investigated powders. The highest circularity was measured for the PREP powders, which had a circularity of up to 0.99, whereas the lowest circularity was measured for the WA powder, which had a circularity of 0.68. Most GA powders have a circularity of approximately 0.9. The aspect ratio was lower than the circularity for all powders. The absolute values of the circularity and aspect ratio were within the range of what has been reported in the literature for the respective production processes [11,25–29]. Furthermore, the results showed a strong correlation between powder circularity and aspect ratio with a Pearson correlation coefficient (PCC) of $r$ (12) = 0.91, $p < 0.001$. Thus, subsequently, only circularity will be discussed as all dependencies are qualitatively interchangeable for circularity and aspect ratio.

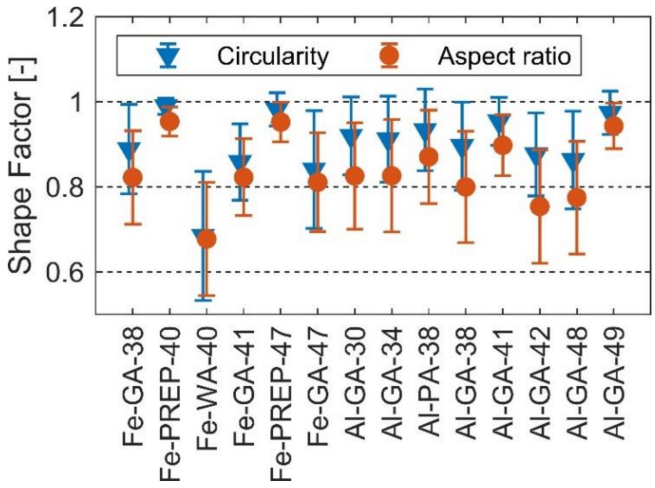


**Figure 4.** The mean circularity and mean aspect ratio of all powders with standard deviation.

### 3.2. Powder Layer Density, Tap Density, and Apparent Density

The PLD, tap density, and apparent density of all powders is displayed in Figure 5. For all powders, the PLD in the 84.5 µm cavity was lower than in the 141.4 µm cavity, and both PLDs were lower than the apparent density of the powders. This was due to the wall effect, which is the reduction of packing density through vacant sites in a packed powder in the presence of a wall, as discussed in [29,30]. For a solid material layer with a height of 30 µm, recent studies indicate that 141.1 µm is close to the realistic effective powder layer thickness for the LPBF process; Wischeropp et al. [6] measured it to be between 130 and 165 µm. These results are supported by the recent findings of Mahmoodkhani et al. [7], who measured the effective powder layer thickness to be greater than 100 µm in all of their experiments. Therefore, the subsequent discussion is mostly based on the PLD of the 141.4 µm cavity, which is more representative of the reality.

The measured PLDs for the 141.1 µm cavity are comparable to values in the literature, i.e., those of Wischeropp et al. [6], who measured the PLD to be between 44% and 53% for three LPBF powders, and Chen et al. [31], who measured a PLD for a single layer of 316L powder to be approx. 45% for a coating speed of 100 mm/s. The water-atomized powder Fe-WA-40, which was the least spherical, exhibited the lowest PLD, whereas the PREP powders, which were the most spherical ones, exhibited the highest layer densities. This trend will be discussed in more detail in the following sections.

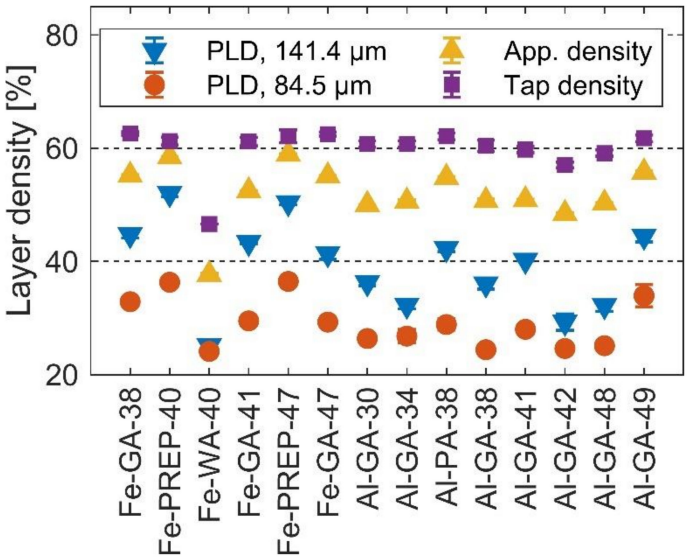


**Figure 5.** The mean powder layer density (PLD) for both cavities, apparent density, and tap density of all powders as a fraction of the full material density with standard deviation.

### 3.3. Hausner Ratio

The Hausner ratios of all powders are displayed in Figure 6, as calculated from the tap and apparent density in Figure 5. The values range from 1.05 for Fe-PREP-40 to 1.24 for Fe-WA-40. According to Sutton et al. [32], any powder with a Hausner ratio below 1.25 can be considered free-flowing, which is in accordance with the subjective perception of the powder flow of all powders. All powders had sufficient flowability to be processed on a LPBF machine, yet did not necessarily yield sufficient part quality, as it will be subsequently shown. The Hausner ratios were within the range of what has been reported in the literature for similar powders; i.e., approx. 1.17 for GA AlSi10Mg in [11], approx. 1.11 for PA AlSi10Mg in [11], a variety of Fe and Ni powders for LPBF with Hausner ratios mostly between 1.1 and 1.2 in [5], water-atomized 316L powder with 1.27 in [28], and others in [3,33].

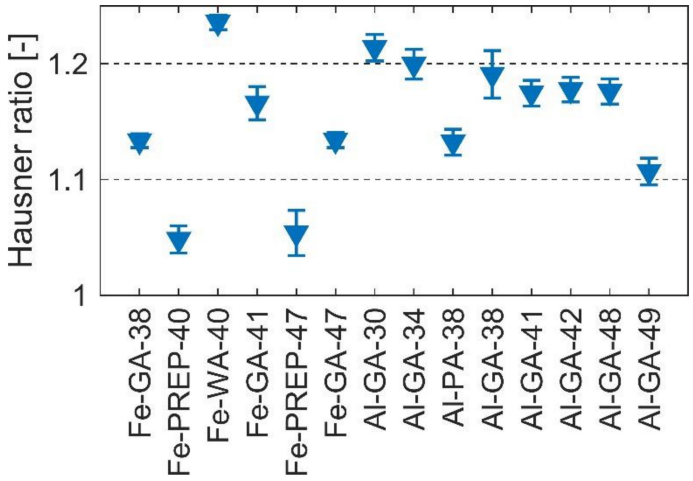


**Figure 6.** The mean Hausner ratio of all powders with standard deviation.

### *3.4. Relationship between PLD, Circularity, and Hausner Ratio*

Figure 7 shows the relationship between PLD for both cavities, circularity, and Hausner ratio. The PLD for the 141.4 µm-deep cavity is plotted against the PLD of the 84.5 µm-deep cavity in Figure 7a. Besides the fact that the PLD was higher for the deeper cavity for every single powder, there was a linear relation with a PCC of $r$ (12) = 0.92, $p < 0.001$ between the mean PLD for the 84.5 µm and 141.4 µm cavities. The PLD is plotted against the mean circularity in Figure 7b and shows a linear dependency between the PLD and the powder circularity with a PCC of $r$ (12) = 0.72 $p < 0.01$. Furthermore, this trend seems dependent on the material, as the layer density values for AlSi10Mg powders were lower than those for 1.4404 (316L) powders for the same circularity.

The Hausner ratio is plotted against the mean circularity in Figure 7c. The data show a moderate linear correlation with a PCC of $r$ (12) = −0.67, $p < 0.01$ for the combined 1.4404 (316L) and AlSi10Mg data. However, the dependence of Hausner ratios on circularity, just like that of PLD on circularity, seems to be material-dependent, as the Hausner ratio for AlSi10Mg powders was higher for the same circularity. The dependency of the Hausner ratio on the particle shape has been shown in [34], where the Hausner ratio increases for decreasing particle sphericity. There was also a linear relationship between the PLD for the 141.4 µm cavity and the Hausner ratio with a PCC of $r$ (12) = –0.89, $p < 0.001$, as shown in Figure 7c. This trend, in contrast to the Hausner ratio and PLD, fits the data for both 1.4404 (316L) and AlSi10Mg powders independent of the material.

In summary, the PLD in both cavities correlated strongly. The PLD and Hausner ratio of a powder cannot be predicted only from its circularity, as they seem to be material-dependent. The Hausner ratio, however, is a good predictor for the PLD in LPBF and did not show a material dependency for the two alloys in this experiment. As the Hausner ratio depends on the friction between powder particles [35], caused by either particle shape, oxides, or other factors, it seems that low friction between the powder particles caused a higher PLD. This finding is also supported by the fact that the Al powders in Figure 7c exhibited a higher Hausner ratio than the Fe powders for the same circularity, which in turn caused the lower PLD of Al powders for the same circularity in Figure 7b.

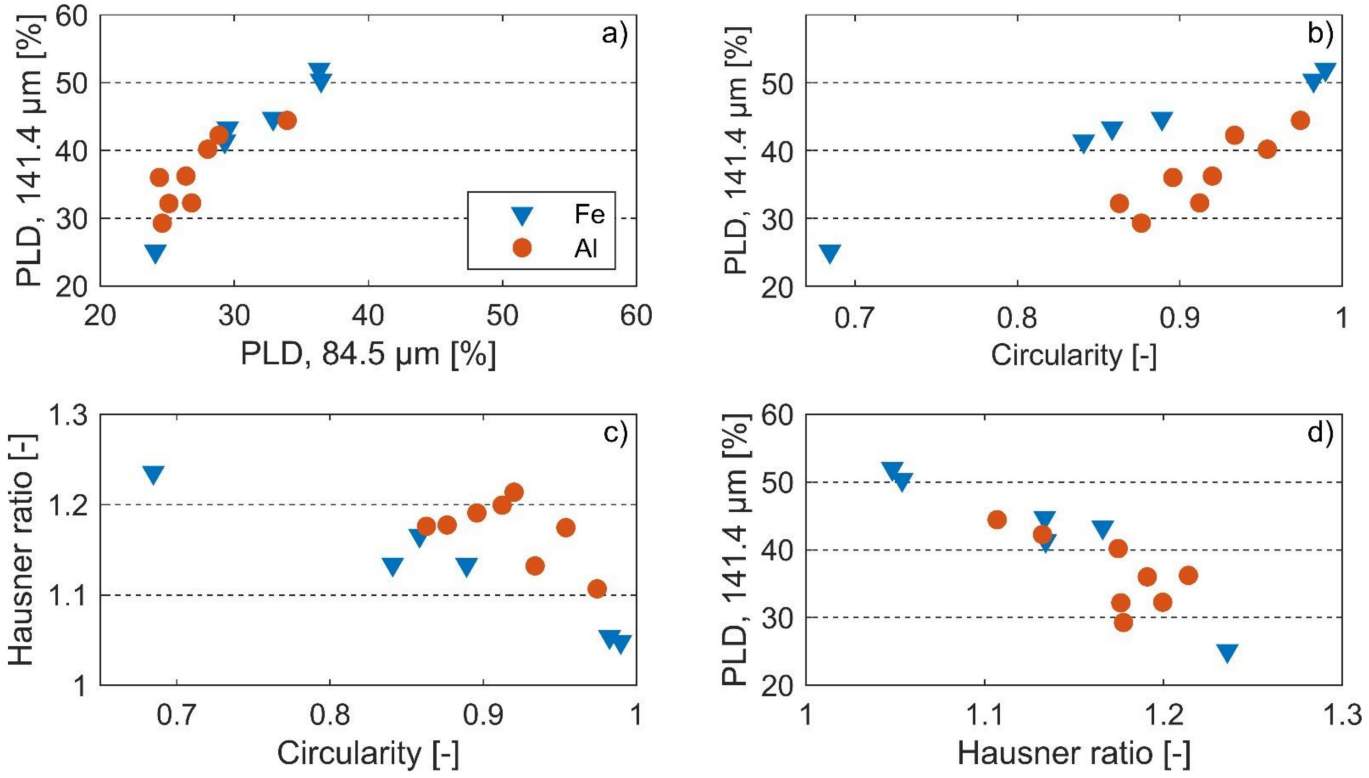


**Figure 7.** The correlation between: (**a**) mean PLD for the 141.4 µm and 84.5 µm cavity, (**b**) mean PLD for the 141.4 µm cavity and mean circularity, (**c**) Hausner ratio and mean circularity, and (**d**) PLD for the 141.4 µm cavity and Hausner ratio.

### *3.5. Part Density*

All powders were processed on an LPBF machine with parameters reported in Section 2.3. The material density of parts made from every powder at five scan speeds is displayed in Figure 8 for (a) 1.4404 (316L) and (b) AlSi10Mg. Some of the cubes from the Fe-WA-40 powder showed delamination issues, as displayed in Figure 9. The density of these cubes was omitted from the data as it is affected by the porosity due to delamination.

The part density decreases, as typical for LPBF [36,37], with increasing scan speed for all powders. While the processing windows of Fe-GA-38, Fe-PREP-40, and Fe-GA-41 in Figure 8a were similar, the other three 14404 (316L) powders exhibited a different processing window. PREP-47 and Fe-GA-47 exhibited a similar processing window with a high decrease in part densities for scan speeds higher than 1250 mm/s. This can be explained by their coarser PSD, as Meiners [37] and Simchi [38,39] observed before and showed that coarser powders lead to increased part porosity at high scan speeds. The processing window of the water-atomized Fe-WA-40 differed from those of all other powders. For all scan speeds, the part density of parts made from WA powder was almost 2 percentage points lower than of parts made from gas-atomized and PREP powders with similar PSD. This high porosity in parts made from water-atomized powder in LPBF is widely known [3,9,14]; however, Hoeges et al. [10] demonstrated the processing of water-atomized 316L with densities of more than 99% by using adapted processing parameters.

Most density curves for the AlSi10Mg powders in Figure 8b only differed slightly. The exception is the processing window of AL-GA-48, which was approx. 1 percentage point lower than the processing window of the other powders. One contributor to the lower density is the coarser PSD, which has been shown to cause porosity in parts [37–39]. Surprisingly, the processing window of Al-GA-49 was similar to those of the finer powders. This might be explained by its circularity, which is the highest among the Al powders. The Al powder with the second-highest circularity, Al-GA-41, however, did not yield parts with a higher density than Al powders with a similar PSD. Therefore, the positive influence of

circularity on part density cannot be concluded for all powders. These findings will be discussed in the next sections.

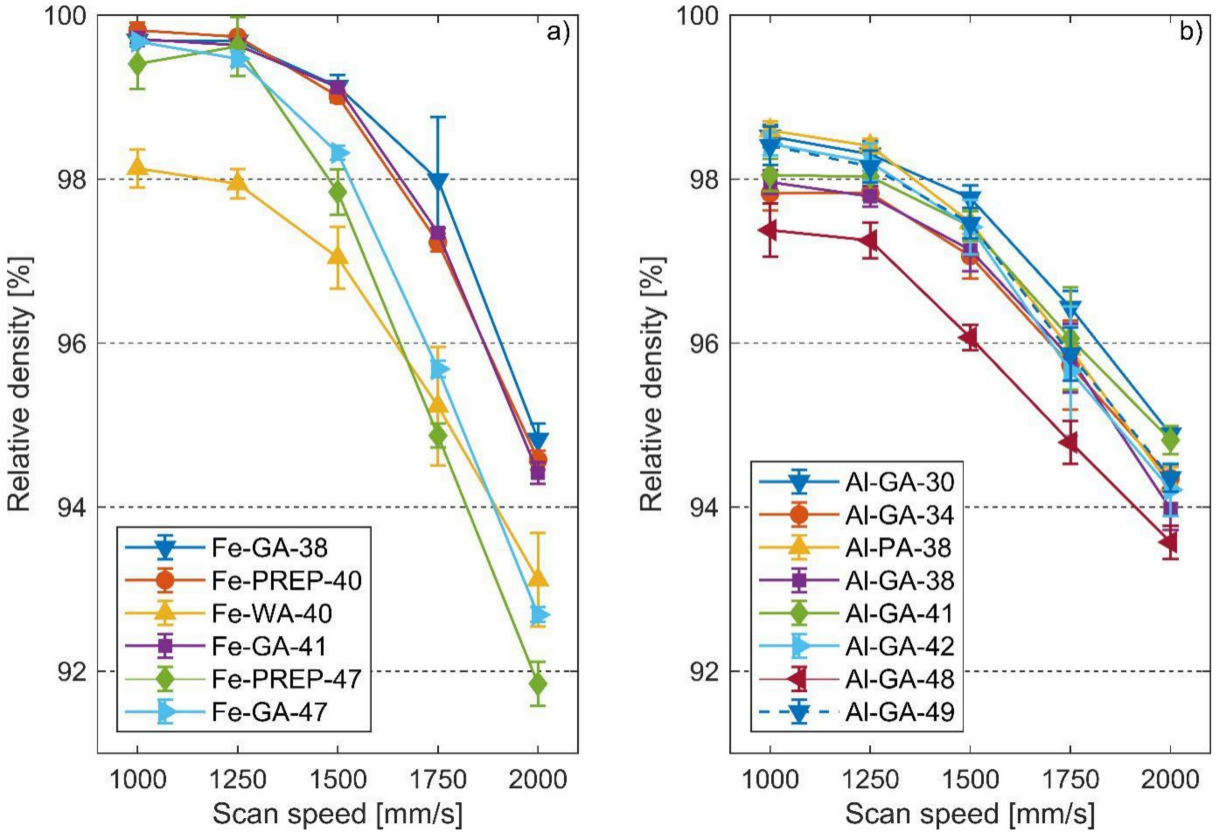


**Figure 8.** The dependency of the mean material density and its standard deviation on the scan speed of (**a**) 1.4404 (316L) and (**b**) AlSi10Mg for all powders.

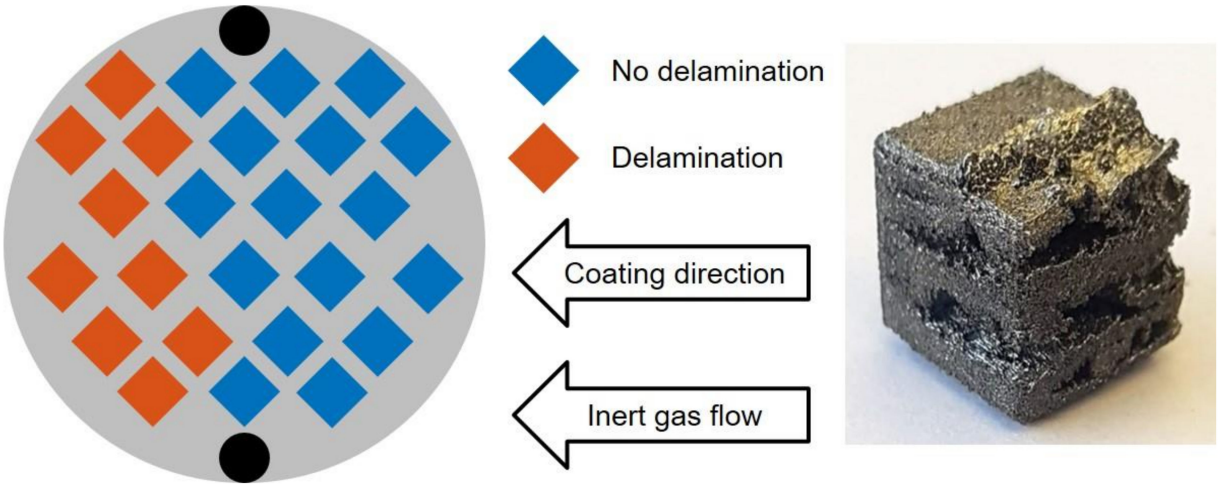


**Figure 9.** Delamination of the cubes built from the WA powder and a cube with delamination issues.

### *3.6. Dependence of the Part Density on the Particle Circularity*

To identify causes for part porosity, the density data in Figure 8 is analyzed in more detail in this section. Figure 10 shows the mean part porosity plotted against powder circularity at scan speeds of 1000, 1500, and 2000 mm/s. All powders with D50 > 45 µm are shown in non-solid symbols. This is done to set them apart from the other powders, as their part porosity can be higher than the porosity of parts made from finer powders, as shown

in [37–39]. The data show a difference in part densities between AlSi10Mg and 1.4404 (316L). At 1000 and 1500 mm/s, the porosity of the AlSi10Mg parts was approximately 1.5 percentage points higher for powders with D50 < 45 µm, the WA powder not considered. This was due to the material dependency of the processing windows for LPBF.

Furthermore, the data show that, except for Fe-WA-40, there was no influence of circularity on part density for both materials. Only the WA powder, which had the lowest circularity of all powders, showed a lower part density compared to powders made from the same alloy and with a similar PSD. The data for the four powders with a D50 > 45 µm also indicated no relationship between the part density and powder circularity.

The high part porosity of parts made from water-atomized powder has been shown before [3,9,12]. The finding for the other powders are in contrast to the results of Riener et al. [11], who compared three GA powders and one PA AlSi10Mg powder and Brika et al. [12], who compared one GA powders and two PA Ti-6Al-4V powders. Both found that more spherical particles lead to higher part density. Other authors report similar findings as in this experiment; i.e., little differences in part density for different particle shapes; e.g., Seyda, Herzog, and Emmelmann [40] found little difference in part density for three Ti-6Al-4V powders despite differences in particle morphology.

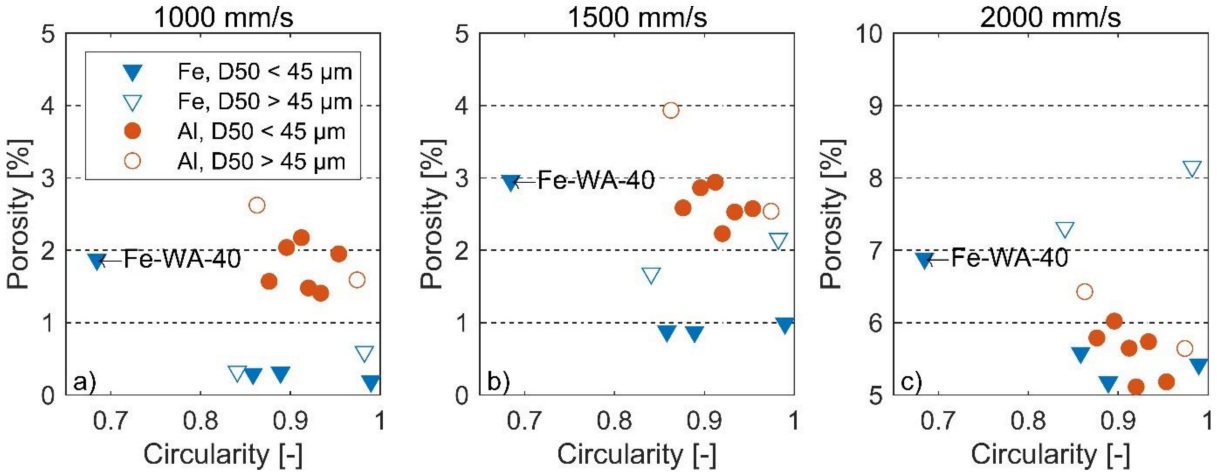


**Figure 10.** Mean part porosity plotted against the mean powder circularity for a scan speed of (**a**) 1000 mm/s, (**b**) 1500 mm/s, and (**c**) 2000 mm/s. The y-axis of graph (**c**) differs from that of graphs (**a**,**b**).

### *3.7. Dependence of the Part Density on the Hausner Ratio*

Figure 11 shows the mean part porosity plotted against the Hausner ratio at scan speeds of 1000, 1500, and 2000 mm/s. The results once again show, except for Fe-Wa-40, that there was no clear influence of the Hausner ratio on part density. Since the Hausner ratio correlated with the particle circularity (compare Figure 7c) and the circularity of any but the water-atomized powder did not predict the part density, the Hausner ratio consequently also did not predict part porosity.

These findings are in contrast to the results of Engeli et al. [3], who found a relationship between the Hausner ratio and part density in LPBF for eight IN738LC powders. Brika et al. [12] also analyzed three powders, of which the one with the lowest Hausner ratio yielded parts with the lowest density, and Riener et al. [11] found in a comparison of three Ti-6Al-4V powders that the powder with the lowest Hausner ratio yielded parts with the highest density.

Powder with a too low flowability is undoubtedly unsuited for LPBF [5,41]. It is likely that the low flowability of the water-atomized Fe-WA-40 powder caused the low part porosity and also the delamination shown in Figure 9. It might, however, be that a decrease of the Hausner ratio of a powder beyond a certain threshold generated no further improvement of processability. This was also concluded by Pleass and Jothi [41], whose

findings indicate that once adequate flowability is achieved, the processing parameters become much more relevant for part quality.

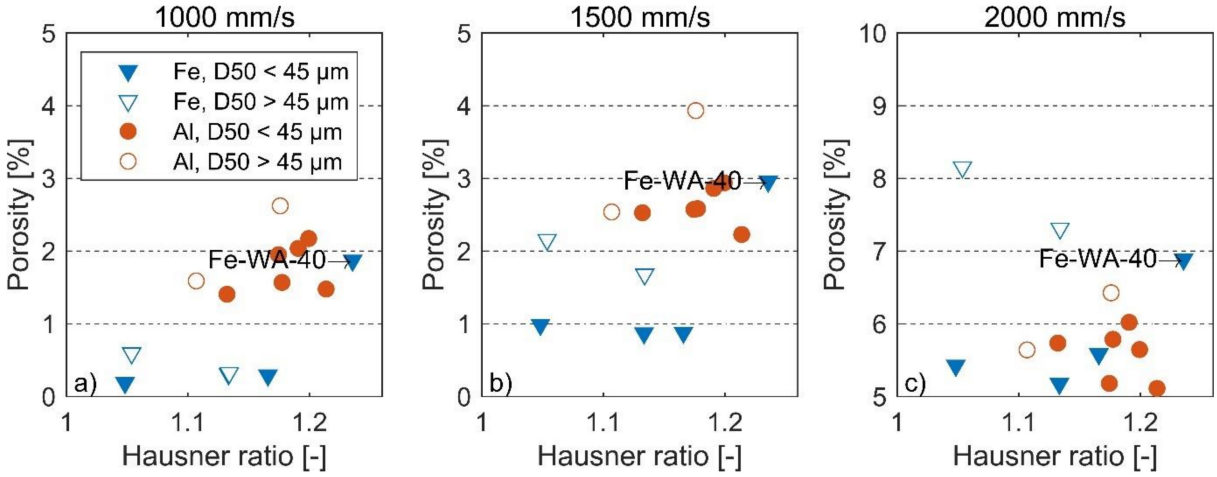


**Figure 11.** Mean part porosity against the Hausner ratio for a scan speed of (**a**) 1000 mm/s, (**b**) 1500 mm/s, and (**c**) 2000 mm/s. The y-axis of graph (**c**) differs from that of graphs (**a**,**b**).

### *3.8. Dependence of the Part Density on the Powder Layer Density*

As the circularity and the Hausner ratio seemed to impact only the part density for WA powder, the influence of PLD on part density is evaluated in this section as the relevance of a high PLD for part quality is frequently stressed in literature [5,32,41,42]. Figure 12 shows the mean part porosity plotted against the PLD at scan speeds of 1000, 1500, and 2000 mm/s. The data show that, except for the Fe-Wa-40 powder and a material-dependent difference between Al and Fe powders, there was no influence of the PLD on the part density for either AlSi10Mg or 1.4404 (316L).

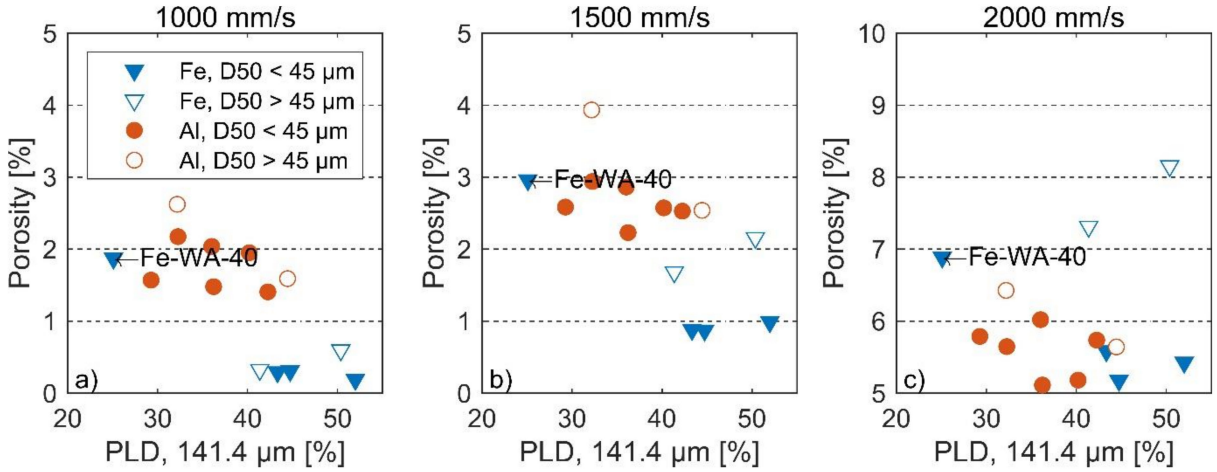


**Figure 12.** Mean part porosity against the PLD for the 141.4 µm cavity for a scan speed of (**a**) 1000 mm/s, (**b**) 1500 mm/s, and (**c**) 2000 mm/s. The y-axis of graph (**c**) differs from that of graphs (**a**,**b**).

An explanation for the limited impact of the PLD on the part density is given by the denudation of metal powder during LPBF, as has been described by Matthews et al. [43] and Bidare et al. [44]. Matthews et al. [43] showed that the metal vapor flux of the melt pool causes a shear gas flow, which entraps adjacent particles. The particles are then rearranged before the laser passes again and interacts with them. Consequently, the laser and melt pool do not interact with the powder bed as it has been deposited, but only with the rearranged particles. Furthermore, the law of conservation of mass causes the mass of

the deposited powder to be the same as the mass of a solidified layer for the steady state, which is, as discussed in [45], reached after approximately seven layers. This makes the process, in contrast to other powder bed-based processes, less sensitive for variation in the PLD and powder layer homogeneity. Only when the flowability of a powder falls short of a minimal threshold does the powder bed become too inhomogeneous so that defects cannot be compensated for by the movement of particles in the shear gas flow, which then causes porosity, as is the case for the water-atomized Fe-WA-40 powder.

## 4. Conclusions

The results show a correlation between the particle shape, powder flowability, and PLD for the investigated powders. The more spherical the powders, the better their flowability, measured by the Hausner ratio. The flowability also directly affected the layer density, as better flowing powders generated layers with higher densities.

The WA powder, with a low circularity, exhibited an insufficient flowability, which caused low PLD, delamination, and part porosity. More spherical powders, such as the GA ones, showed better flowability and yielded parts with much lower porosity. Any improvement of the particle circularity beyond 0.8 did, however, have no positive influence on the part density. The more spherical, e.g., PREP, powders did exhibit better flowability, which resulted in a higher PLD. The increase in PLD did, however, not positively influence the part density. An explanation is given by the movement of powder particles in the shear gas flow. The laser and melt pool do not interact with the powder layer as it is deposited, but the particles are rearranged in the denudation zone of the previous, adjacent, scan track. This makes the LPBF less sensitive to inhomogeneity of the powder layer and particle circularity.

Future work should be done to measure the PLD in situ, as the results presented in this study might deviate from the true PLD. Furthermore, the influence of powder characteristics on other part quality metrics, such as the surface quality and mechanical properties, should be investigated in future experiments with a wider range of processing conditions.

**Author Contributions:** Conceptualization, L.H. (Lukas Haferkamp) and K.W.; methodology, L.H. (Lukas Haferkamp), A.S., K.R., S.Z., G.J.L.; formal analysis, L.H. (Lukas Haferkamp); investigation, L.H. (Lukas Haferkamp), L.H. (Livia Haudenschild); resources, K.W., K.R., S.Z., G.J.L.; writing—original draft preparation, L.H. (Lukas Haferkamp); writing—review and editing, L.H. (Lukas Haferkamp) and K.R.; visualization, L.H. (Lukas Haferkamp); supervision, K.W.; project administration, L.H. (Lukas Haferkamp). All authors have read and agreed to the published version of the manuscript.

**Funding:** This research received no external funding.

**Institutional Review Board Statement:** Not applicable.

**Informed Consent Statement:** Not applicable.

**Data Availability Statement:** The data presented in this study are available on request from the corresponding author.

**Conflicts of Interest:** The authors declare no conflict of interest.

## References

1. Sames, W.J.; List, F.A.; Pannala, S.; Dehoff, R.R.; Babu, S.S. The metallurgy and processing science of metal additive manufacturing. *Int. Mater. Rev.* **2016**, *61*, 315–360. [CrossRef]
2. Tan, J.H.; Wong, W.L.E.; Dalgarno, K.W. An overview of powder granulometry on feedstock and part performance in the selective laser melting process. *Addit. Manuf.* **2017**, *18*, 228–255. [CrossRef]
3. Engeli, R.; Etter, T.; Hövel, S.; Wegener, K. Processability of different IN738LC powder batches by selective laser melting. *J. Mater. Process. Technol.* **2016**, *229*, 484–491. [CrossRef]
4. Slotwinski, J.A.; Garboczi, E.J. Metrology Needs for Metal Additive Manufacturing Powders. *J. Mater.* **2015**, *67*, 538–543. [CrossRef]
5. Spierings, A.B.; Voegtlin, M.; Bauer, T.; Wegener, K. Powder flowability characterisation methodology for powder-bed-based metal additive manufacturing. *Prog. Addit. Manuf.* **2016**, *1*, 9–20. [CrossRef]

6. Wischeropp, T.M.; Emmelmann, C.; Brandt, M.; Pateras, A. Measurement of actual powder layer height and packing density in a single layer in selective laser melting. *Addit. Manuf.* **2019**, *28*, 176–183. [CrossRef]
7. Mahmoodkhani, Y.; Ali, U.; Imani Shahabad, S.; Rani Kasinathan, A.; Esmaeilizadeh, R.; Keshavarzkermani, A.; Marzbanrad, E.; Toyserkani, E. On the measurement of effective powder layer thickness in laser powder-bed fusion additive manufacturing of metals. *Prog. Addit. Manuf.* **2019**, *4*, 109–116. [CrossRef]
8. Anatoliy, P.; Vadim, S. Metal Powder Additive Manufacturing. *New Trends 3D Print.* **2015**. [CrossRef]
9. Li, R.; Shi, Y.; Wang, Z.; Wang, L.; Liu, J.; Jiang, W. Densification behavior of gas and water atomized 316L stainless steel powder during selective laser melting. *Appl. Surf. Sci.* **2010**, *256*, 4350–4356. [CrossRef]
10. Hoeges, S.; Zwiren, A.; Schade, C. Additive manufacturing using water atomized steel powders. *Met. Powder Rep.* **2017**, *72*, 111–117. [CrossRef]
11. Riener, K.; Albrecht, N.; Ziegelmeier, S.; Ramakrishnan, R.; Haferkamp, L.; Spierings, A.B.; Leichtfried, G.J. Influence of particle size distribution and morphology on the properties of the powder feedstock as well as of AlSi10Mg parts produced by laser powder bed fusion (LPBF). *Addit. Manuf.* **2020**, *34*, 101286. [CrossRef]
12. Brika, S.E.; Letenneur, M.; Dion, C.A.; Brailovski, V. Influence of particle morphology and size distribution on the powder flowability and laser powder bed fusion manufacturability of Ti-6Al-4V alloy. *Addit. Manuf.* **2019**. [CrossRef]
13. Baitimerov, R.; Lykov, P.; Zherebtsov, D.; Radionova, L.; Shultc, A.; Prashanth, K.G. Influence of Powder Characteristics on Processability of AlSi12 Alloy Fabricated by Selective Laser Melting. *Materials* **2018**, *11*, 742. [CrossRef] [PubMed]
14. Irrinki, H.; Dexter, M.; Barmore, B.; Enneti, R.; Pasebani, S.; Badwe, S.; Stitzel, J.; Malhotra, R.; Atre, S.V. Effects of Powder Attributes and Laser Powder Bed Fusion (L-PBF) Process Conditions on the Densification and Mechanical Properties of 17-4 PH Stainless Steel. *J. Mater.* **2016**, *68*, 860–868. [CrossRef]
15. Jeon, T.J.; Hwang, T.W.; Yun, H.J.; VanTyne, C.J.; Moon, Y.H. Control of Porosity in Parts Produced by a Direct Laser Melting Process. *Appl. Sci.* **2018**, *8*, 2573. [CrossRef]
16. Seyda, V. *Werkstoff- und Prozessverhalten von Metallpulvern in der Laseradditiven Fertigung*; Springer: Berlin/Heidelberg, Germany, 2018. [CrossRef]
17. Cooke, A.; Slotwinski, J. *Properties of Metal Powders for Additive Manufacturing: A Review of the State of the Art of Metal Powder Property Testing*; US Department of Commerce, National Institute of Standards and Technology: Gaithersburg, MD, USA, 2012.
18. Gorji, N.E.; O'Connor, R.; Brabazon, D. X-ray Tomography, AFM and Nanoindentation Measurements for Recyclability Analysis of 316L Powders in 3D Printing Process. *Procedia Manuf.* **2020**, *47*, 1113–1116. [CrossRef]
19. Riener, K.; Oswald, S.; Winkler, M.; Leichtfried, G.J. Influence of storage conditions and reconditioning of AlSi10Mg powder on the quality of parts produced by laser powder bed fusion (LPBF). *Addit. Manuf.* **2021**, *39*, 101896. [CrossRef]
20. Bouwman, A.M.; Bosma, J.C.; Vonk, P.; Wesselingh, J.A.; Frijlink, H.W. Which shape factor(s) best describe granules? *Powder Technol.* **2004**, *146*, 66–72. [CrossRef]
21. ASTM. *ASTM B417—18, Standard Test Method for Apparent Density of Non-Free-Flowing Metal Powders Using the Carney Funnel*; ASTM: West Conshohocken, PA, USA, 2018. [CrossRef]
22. ASTM. *B527-15 Standard Test Method for Tap Density of Metal Powders and Compounds*; ASTM: West Conshohocken, PA, USA, 2015. [CrossRef]
23. Spierings, A.; Schneider, M.; Eggenberger, R. Comparison of Density Measurement Techniques for Additive Manufactured Metallic Parts. *Rapid Prototyp. J.* **2011**, *17*, 380–386. [CrossRef]
24. Mugica, G.W.; Tovio, D.O.; Cuyas, J.C.; González, A.C. Effect of porosity on the tensile properties of low ductility aluminum alloys. *Mater. Res.* **2004**, *7*, 221–229. [CrossRef]
25. Kiani, P.; Scipioni Bertoli, U.; Dupuy, A.D.; Ma, K.; Schoenung, J.M. A Statistical Analysis of Powder Flowability in Metal Additive Manufacturing. *Adv. Eng. Mater.* **2020**, *22*, 2000022. [CrossRef]
26. Uhlenwinkel, V.; Schwenck, D.; Ellendt, N.; Fischer-Bühner, J.; Hofmann, P. Gas recirculation affects the powder quality. In Proceedings of the Advances in Powder Metallurgy and Particulate Materials—2014, 2014 World Congress on Powder Metallurgy and Particulate Materials, PM, Orlando, FL, USA, 18–22 May 2014; pp. 246–253.
27. Snow, Z.; Martukanitz, R.; Joshi, S. On the development of powder spreadability metrics and feedstock requirements for powder bed fusion additive manufacturing. *Addit. Manuf.* **2019**, *28*, 78–86. [CrossRef]
28. Inaekyan, K.; Paserin, V.; Bailon-Poujol, I.; Brailovski, V. Binder-Jetting Additive Manufacturing with Water Atomized Iron Powders. In Proceedings of the AMPM 2016 Conference on Additive Manufacturing, Boston, MA, USA, 5–7 June 2016.
29. Haferkamp, L.; Spierings, A.; Rusch, M.; Jermann, D.; Spurek, M.A.; Wegener, K. Effect of Particle size of monomodal 316L powder on powder layer density in powder bed fusion. *Prog. Addit. Manuf.* **2020**. [CrossRef]
30. Karapatis, N.P.; Egger, G.; Gygax, P.E.; Glardon, R. Optimization of powder layer density in selective laser sintering. In Proceedings of the 10th Solid Freeform Fabrication Symposium (SFF), Austin, TX, USA, 9–11 August 1999.
31. Chen, H.; Chen, Y.; Liu, Y.; Wei, Q.; Shi, Y.; Yan, W. Packing quality of powder layer during counter-rolling-type powder spreading process in additive manufacturing. *Int. J. Mach. Tools Manuf.* **2020**, *153*, 103553. [CrossRef]
32. Sutton, A.T.; Kriewall, C.S.; Leu, M.C.; Newkirk, J.W. Powder characterisation techniques and effects of powder characteristics on part properties in powder-bed fusion processes. *Virtual Phys. Prototyp.* **2017**, *12*, 3–29. [CrossRef]
33. Coe, H.G.; Pasebani, S. Use of bimodal particle size distribution in selective laser melting of 316L stainless steel. *J. Manuf. Mater. Process.* **2020**, *4*, 8. [CrossRef]

34. Guo, A.; Beddow, J.K.; Vetter, A.F. A simple relationship between particle shape effects and density, flow rate and Hausner Ratio. *Powder Technol.* **1985**, *43*, 279–284. [CrossRef]
35. Abdullah, E.C.; Geldart, D. The use of bulk density measurements as flowability indicators. *Powder Technol.* **1999**, *102*, 151–165. [CrossRef]
36. Qiu, C.; Panwisawas, C.; Ward, M.; Basoalto, H.C.; Brooks, J.W.; Attallah, M.M. On the role of melt flow into the surface structure and porosity development during selective laser melting. *Acta Mater.* **2015**, *96*, 72–79. [CrossRef]
37. Meiners, W. Direktes Selektives Laser Sintern Einkomponentiger Metallischer Werkstoffe. Ph.D. Thesis, RWTH Aachen, Aachen, Germany, 1999.
38. Simchi, A. The role of particle size on the laser sintering of iron powder. *Metall. Mater. Trans. B* **2004**, *35*, 937–948. [CrossRef]
39. Simchi, A. Direct laser sintering of metal powders: Mechanism, kinetics and microstructural features. *Mater. Sci. Eng. A* **2006**, *428*, 148–158. [CrossRef]
40. Seyda, V.; Herzog, D.; Emmelmann, C. Relationship between powder characteristics and part properties in laser beam melting of Ti–6Al–4V, and implications on quality. *J. Laser Appl.* **2017**, *29*, 022311. [CrossRef]
41. Pleass, C.; Jothi, S. Influence of powder characteristics and additive manufacturing process parameters on the microstructure and mechanical behaviour of Inconel 625 fabricated by Selective Laser Melting. *Addit. Manuf.* **2018**, *24*, 419–431. [CrossRef]
42. Balbaa, M.A.; Ghasemi, A.; Fereiduni, E.; Elbestawi, M.A.; Jadhav, S.D.; Kruth, J.P. Role of powder particle size on laser powder bed fusion processability of AlSi10mg alloy. *Addit. Manuf.* **2020**. [CrossRef]
43. Matthews, M.J.; Guss, G.; Khairallah, S.A.; Rubenchik, A.M.; Depond, P.J.; King, W.E. Denudation of metal powder layers in laser powder bed fusion processes. *Acta Mater.* **2016**, *114*, 33–42. [CrossRef]
44. Bidare, P.; Bitharas, I.; Ward, R.M.; Attallah, M.M.; Moore, A.J. Fluid and particle dynamics in laser powder bed fusion. *Acta Mater.* **2018**, *142*, 107–120. [CrossRef]
45. Spierings, A.B.; Levy, G. Comparison of density of stainless steel 316L parts produced with selective laser melting using different powder grades. In Proceedings of the Solid freeform fabrication Symposium, Austin, TX, USA, 3–5 August 2009; pp. 342–353.